Intelligent control of a DC microgrid consisting of Wave Energy Converter (WEC) and Hybrid Energy Storage System (HESS)

Hafiz Ahsan Said, and John V. Ringwood

***Abstract*—Greater efficiency, and the relatively more straightforward structure of DC microgrids, give rise to DC microgrid technology for renewable energy integration. In this work, an intelligent controller is proposed for a DC microgrid that comprises a wave energy converter and a hybrid energy storage system. A wave energy converter oscillating in heave, which drives a linear permanent magnet generator as a power take-off (PTO) mechanism, is used in this study. Additionally, HESS, consisting of battery and supercapacitor, is used for power quality improvement and DC bus voltage regulation. The DC bus connects with each system component through dedicated power converters, with the WEC device using an active rectifier, and the HESS (battery and ultra-capacitor) utilising two bidirectional DC-DC converters. In the paper, a model is derived for the individual components of the microgrid. Then, Lyapunov-based intelligent controllers are designed for the power converters in such a way that they achieve the control objectives. An energy management strategy is also used to ensure proper power-sharing among the HESS components. The controller system is then simulated in a MATLAB/Simulink environment, and the result shows that the proposed controllers achieve the desired control objectives and perform well under various operating conditions.**

***Index Terms*—DC microgrid, Hybrid energy storage, Lyapunov control, Power converters, Wave energy**

I. Introduction

RENEWABLE energy integration is vital in overcoming the environmental impact of tradition fossil fuel plants. The inherent intermittency of renewable energy sources (RESs), such as wave and wind, cause problems for modern electricity grids, especially at higher penetration levels. Renewable energy-based distributed generation (DG) is a viable solution to mitigate the negative impacts of increased RES penetration into national power grids [1]. The concept of DC microgrids for DG is gaining popularity for the following reasons: increased penetration of modern DC loads (motor drives and computing devices etc.), broad utilisation of energy storage (batteries and supercapacitors etc.) and less power quality issues, compared to AC microgrids [2], [3]. DC microgrids are therefore considered to be an integral part of future smart grids.

This work is supported by COER and the Dept. of Electronic Engineering, Maynooth University, and by Science Foundation Ireland through the Marine Renewable Ireland (MaREI) Centre under Grant 12/RC/2302.

Hafiz Ahsan Said and John V. Ringwood are with the Centre for Ocean Energy Research (COER), Maynooth University, Maynooth, Ireland (e-mail: hafiz.said.2020@mumail.ie, john.ringwood@mu.ie).

Wave energy provides a vast potential for clean energy and will be instrumental in the transition towards a 100% renewable future. Many wave energy converters (WECs) have been developed over the past few years to harness the wave energy resource [4]. Like other RESs, the wave energy resource is intermittent, relatively unpredictable and highly variable, which poses a significant challenge for grid integration. Some of the impacts of wave energy on the existing grids include load mismatch, low power quality, frequency deviations and reliability issues [5]–[7]. It is necessary to tackle the problems mentioned above to increase wave energy penetration into power grids. One possible solution is using an energy storage system (ESS), which improves power quality and stores surplus energy. Ideally, an ESS should have high power and energy densities for increased operational flexibility. Therefore, the most frequently utilised (battery) energy storage system (BESS) is not, in general, the right choice for wave energy grid integration due to its low power density. Instead, a combination of two disparate storage technologies, such as a battery-super capacitor (SC) combination, is preferred to achieve simultaneous high power and energy densities. Such a combination is known as a hybrid energy storage system (HESS). The complementary nature of Battery-SC based HESS provides high energy density, high power density, fast dynamic response, and increased lifetime [8]–[10]. Appropriate control of the associated power converters is also crucial for grid integration. However, grid integration studies, involving wave energy, generally have some drawbacks, such as simplified hydrodynamic models, simplified power converter models and relatively rudimentary PI power converter control. Mostly, wave energy grid integration studies use PI control, which can be very sensitive to model parameter variations [11]. A gravitational search algorithm based PI control for a DC microgrid with wave energy as a RES is presented in [12], but the hydrodynamic model of WEC and models of power converters are simplified. Similarly, MPC-based control of a WEC-based DC microgrid is proposed in [13], which shows that MPC performs better than PI control, but the hydrodynamic model is oversimplified in this study as well.

In this paper, a Lyapunov-based nonlinear control strategy is proposed for a DC microgrid with wave energy as a RES. The proposed DC microgrid structure is shown in Fig. 1, consisting of a wave energy con-

version system (a WEC and linear permanent magnet generator) and battery-supercapacitor based HESS. The WEC and linear permanent magnet generator (LPMG) are connected to the DC bus through an active rectifier referred to as a generator-side converter (Gen-SC). In addition, the components of HESS are connected to the DC bus via bidirectional buck-boost converters. Gen-SC control focuses on hydrodynamic control, responsible for maximum power extraction from the waves. The DC/DC converter control objective, for HESS, revolves around power quality improvement through DC bus voltage regulation. Finally, a filter-based energy management strategy for power sharing among HESS components is included.

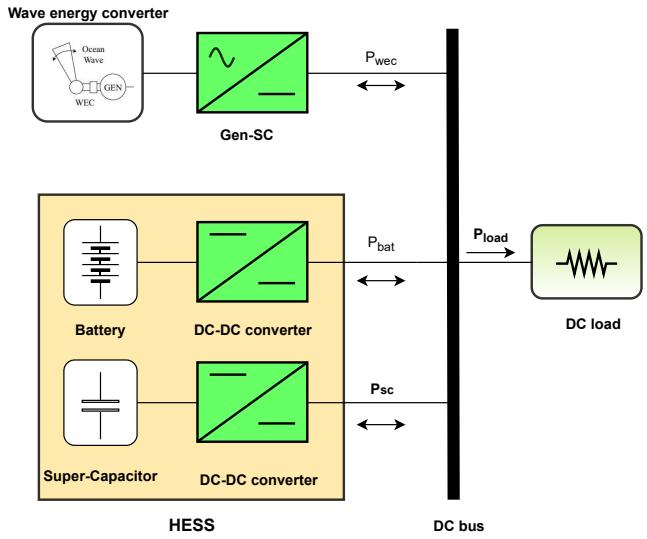

Fig. 1: Proposed DC microgrid

The remainder of the paper is organised as follows: Section II describes the modelling of various components of the DC microgrid, while Section III discusses Lyapunov based control of the power converters. An energy management system is presented in Section IV, with Section V discussing the results of the study. Finally, SectionVI concludes on this study.

II. Modelling of the DC microgrid

A. Modelling of wave energy conversion system in a DC microgrid

The wave energy system comprises a WEC, LPMG and Gen-SC. The modelling of each component is described in the following subsections.

1) WEC model: A single body floating WEC, oscillating in heave, is considered in this study. The dynamics of the WEC in the time domain can be represented by:

$$M\ddot{z}(t) = f_{exc}(t) + f_{pto}(t) + f_r(t) + f_{hs}(t) \tag{1}$$

where, $f_{exc}(t)$, $f_r(t)$ and $f_{hs}(t)$ are the excitation, radiation and hydrostatic forces respectively; $f_{pto}(t)$ represents the force applied by the LPMG on the WEC. M is the total mass of the oscillating system, while $z(t)$, $\dot{z}(t)$ and $\ddot{z}(t)$ represent heave displacement, velocity and acceleration, respectively. We dispense with the time dependence (t) notation, for brevity. The hydrostatic stiffness force is given by:

$$f_{hs} = -K_{hs}z \tag{2}$$

where K_{hs} represents the hydrostatic stiffness. The radiation force f_r is modelled through linear potential flow theory, using Cummins' equation, as follows [14]:

$$f_r = -m_\infty \ddot{z} - K_r * \dot{z}, \tag{3}$$

where, m_∞ is the added mass at infinite frequency, and K_r is the radiation impulse response function. The operator $*$ represents the convolution operator. A finite order parametric approximation for the convolution term $f_{rc} = K_r * \dot{z}$ is calculated using the FOAMM toolbox [15] as follows:

$$\begin{aligned} \dot{Y}_r &= A_r Y_r + B_r \dot{z} \\ f_{rc} &= C_r Y_r \approx K_r * \dot{z} \end{aligned} \tag{4}$$

The excitation force is calculated by the method described by Guo et. al in [16]. Finally, the hydrodynamic model, with state variables vector $\chi(t) = \begin{bmatrix} Y_r & z & \dot{z} \end{bmatrix}^\top$, can be written as:

$$\dot{\chi} = A\chi + Bf_{exc} + Bf_{pto}, \tag{5}$$

with

$$A = \begin{bmatrix} 0 & 1 & 0_{1\times n} \\ -K_{hs}/(M+m_\infty) & 0 & -Cr/(M+m_\infty) \\ 0_{n\times 1} & B_r & A_r \end{bmatrix},$$

$$B = \begin{bmatrix} 0 & 1/(M+m_\infty) & 0_{1\times n} \end{bmatrix}^\top$$

2) LPMG and Gen-SC model: The dynamic model of LPMG in the dq- synchronous frame of reference, moving with electrical angular frequency ω_e, can be written [17] as:

$$\frac{di_d}{dt} = -\frac{R_s}{L_s}i_d + \omega_e i_q - \frac{1}{L_s}v_d \tag{6}$$

$$\frac{di_q}{dt} = -\omega_e i_d - \frac{R_s}{L_s}i_q - \frac{\omega_e}{Ls}\psi_{PM} - \frac{1}{L_s}v_d \tag{7}$$

$$f_{pto} = -1.5\frac{\pi}{\tau}\psi_{PM} i_q \tag{8}$$

where, $v_{d,q}$ and $i_{d,q}$ are the d- and q-axis stator voltages and currents respectively, ψ_{PM} is the permanent magnet flux linkages, L_s and R_s are stator inductance and resistance respectively, and f_{pto} is the generator force acting on the WEC. ω_e is the angular frequency of the stator variables and can be calculated as:

$$\omega_e = \frac{\pi}{\tau}\dot{z} \tag{9}$$

where τ is pole pitch of the LPMG. Since the stator d- and q-axis voltages act as the inputs to Gen-SC and can be controlled independently, these voltages can be expressed in terms of corresponding converter control actions [18], [19] as follows:

$$v_d = v_{dc}u_d; \quad v_q = v_{dc}u_q \quad \text{and} \quad i_{wec} = u_d i_d + u_q i_q \tag{10}$$

where u_d and u_q are the Park transformation of (S_i, $\forall$ $i = 1, 2, 3$) (refer to Fig. 2), with

$$S_i = \begin{cases} 1 & \text{if } S_i \text{ is ON and } S_i' \text{ is OFF} \\ 0 & \text{if } S_i \text{ is OFF and } S_i' \text{ is ON} \end{cases} \tag{11}$$

Putting the values of v_d and v_q from Eq. (10) into Eqs. (6) and (7), we get the following unified generator-rectifier model:

$$\frac{di_d}{dt} = -\frac{R_s}{L_s} i_d + \omega_e i_q - \frac{1}{L_s} v_{dc} u_d \tag{12}$$

$$\frac{di_q}{dt} = -\omega_e i_d - \frac{R_s}{L_s} i_q - \frac{\omega_e}{Ls} \psi_{PM} - \frac{1}{L_s} v_{dc} u_q \tag{13}$$

B. HESS model

Fig. 2 shows the complete schematic of the DC microgrid. Both battery and super-capacitor are connected to the DC bus through buck-boost converters.

1) Battery and buck-boost converter model: The buck-boost converter operates in both boost and buck mode, depending upon the direction of power flow. In discharge mode, the battery supplies power to the microgrid and the converter works as a boost converter (S_4 ON, S_5 OFF). On the other hand, it operates in buck mode during charge mode (S_4 OFF, S_5 ON) and power from the microgrid charges the battery. During discharge mode, the model is easily derived as:

$$\frac{di_{bat}}{dt} = \frac{V_{bat}}{L_{bat}} - \frac{R_{bat}}{L_{bat}} i_{bat} - (1 - u_4) \frac{v_{dc}}{L_{bat}} \tag{14}$$

$$i'_{bat} = (1 - u_4) i_{bat} \tag{15}$$

During charge mode, the model is derived as follows:

$$\frac{di_{bat}}{dt} = \frac{V_{bat}}{L_{bat}} - \frac{R_{bat}}{L_{bat}} i_{bat} - u_5 \frac{v_{dc}}{L_{bat}} \tag{16}$$

$$i'_{bat} = u_5 i_{bat} \tag{17}$$

where, V_{bat}, L_{bat}, and R_{bat} are battery voltage, inductance and equivalent series resistance, i_{bat} and i'_{bat} are battery input and output currents. u_4 and u_5 are control signals for switches S_4 and S_5. For simplicity, a virtual control signal u_{45} is introduced as:

$$u_{45} = M(1 - u_4) + (1 - M) u_5 \tag{18}$$

where M is defined as follows:

$$M = \begin{cases} 1 & \text{if } S_4 \text{ is ON and } S_5 \text{ is OFF (Boost mode)} \\ 0 & \text{if } S_4 \text{ is OFF and } S_5 \text{ is ON (Buck mode)} \end{cases}$$

Finally, the simplified model for the DC/DC converter using the u_{45}, gives:

$$\frac{di_{bat}}{dt} = \frac{V_{bat}}{L_{bat}} - \frac{R_{bat}}{L_{bat}} i_{bat} - u_{45} \frac{v_{dc}}{L_{bat}} \tag{19}$$

$$i'_{bat} = u_{45} i_{bat} \tag{20}$$

2) Supercapacitor (SC) and buck-boost converter model: Similar to the battery model, the SC converter model is derived as follows:

$$\frac{di_{sc}}{dt} = \frac{V_{sc}}{L_{sc}} - \frac{R_{sc}}{L_{sc}} i_{sc} - u_{67} \frac{v_{dc}}{L_{sc}} \tag{21}$$

$$i'_{sc} = u_{67} i_{bat} \tag{22}$$

where u_{67} is the virtual control for SC buck-boost converter and is defined as:

$$u_{67} = K(1 - u_6) + (1 - K) u_7 \tag{23}$$

with K defined as:

$$K = \begin{cases} 1 & \text{if } S_6 \text{ is ON and } S_7 \text{ is OFF (Boost mode)} \\ 0 & \text{if } S_6 \text{ is OFF and } S_7 \text{ is ON (Buck mode)} \end{cases}$$

C. Global DC microgrid model

From Fig. 2, it follows that:

$$C_{dc} \frac{dv_{dc}}{dt} = i_{wec} + i'_{bat} + i'_{sc} - i_{load} \tag{24}$$

Using Eqs. (10), (20) and (22) in Eq. (24) gives:

$$\frac{dv_{dc}}{dt} = \frac{1}{C_{dc}} [(u_d i_d + u_q i_q) + u_{45} i_{bat} + u_{67} i_{sc} - i_{load}] \tag{25}$$

For control design, it is convenient to use averaged models for the converters. In this regard, we define averaged state variables as $x_1 =< i_d >$, $x_2 =< i_q >$, $x_3 =< i_{bat} >$, $x_4 =< i_{sc} >$ and $x_5 =< v_{dc} >$, where the operator $< \bullet >$ represent the average value over a switching period. Combining Eqs. (12), (13), (20), (22) and (25) results in the following global DC microgrid model.

$$\frac{dx_1}{dt} = -\frac{R_s}{L_s} x_1 + \omega_e x_2 - \frac{1}{L_s} x_5 \mu_d \tag{26}$$

$$\frac{dx_2}{dt} = -\omega_e x_1 - \frac{R_s}{L_s} x_2 - \frac{\omega_e}{Ls} \psi_{PM} - \frac{1}{L_s} x_5 \mu_q \tag{27}$$

$$\frac{dx_3}{dt} = \frac{V_{bat}}{L_{bat}} - \frac{R_{bat}}{L_{bat}} x_3 - \mu_{45} \frac{x_5}{L_{bat}} \tag{28}$$

$$\frac{dx_4}{dt} = \frac{V_{sc}}{L_{sc}} - \frac{R_{sc}}{L_{sc}} x_4 - \mu_{67} \frac{x_5}{L_{sc}} \tag{29}$$

$$\frac{dx_5}{dt} = \frac{1}{C_{dc}} [(\mu_d x_1 + \mu_q x_2) + \mu_{45} x_3 + \mu_{67} x_4 - i_{load}] \tag{30}$$

where, μ_d, μ_q, μ_{45} and μ_{67} are the duty ratios of the Gen-SC and HESS converters i.e. the average values of the control inputs u_d, u_q, u_{45} and u_{67}, respectively.

III. Lyapunov based control design

This section is devoted to the design and analysis of the Lyapunov-based control of the DC microgrid power converters. The control objectives for the DC microgrid are summarised as:

1) Maximum power extraction from the waves by tracking a reference PTO force generated through hydrodynamic control.
2) DC bus voltage regulation.
3) Tracking of battery and SC currents to their references.
4) Ensuring asymptotic stability of the microgrid.

A. Control of Gen-SC for WEC maximum power extraction

The first control objective is to extract maximum power from the waves and this is achieved through the control of Gen-SC. This is done in two parts: (i) reference generation, and (ii) controller design for reference tracking.

1) Reference generation (hydrodynamic control): Two hydrodynamic control strategies are used to generate references for Gen-SC control. First, a very simple passive control, also known as resistive loading (RL) control, is used to generate the PTO reference force. Since RL is a passive control, it does not require any reactive power from the microgrid. The PTO reference force f_{pto}^{ref} generated from a RL control [20], [21] is given by:

$$f_{pto}^{ref} = |Z(\omega_{pk})|\dot{z} \tag{31}$$

where,
$|Z(\omega_{pk})| = \sqrt{B(\omega_{pk})^2 + (\omega_{pk}(m + m_{add}(\omega_{pk})) - \frac{K_{hs}}{\omega_{pk}})^2}$
is the optimal PTO resistance at a chosen frequency ω_{pk}, where ω_{pk} is typically the peak of the input wave spectrum. $B(\omega)$ and $m_{add}(\omega)$ are the frequency domain radiation damping and added mass.

Secondly, an approximate complex conjugate (ACC) control is also used for reference generation, which is a causal approximation of reactive control. This strategy allows reactive power to flow from the microgrid to the WEC. Under ACC control, f_{pto}^{ref} is derived as [20], [21]:

$$f_{pto}^{ref} = B(\omega_{pk})\dot{z} + (\omega_{pk}^2(m + m_{add}(\omega_{pk}) - K_{hs}))z \tag{32}$$

f_{pto}^{ref}, from Eqs. (31) and (32), is used to generate current reference for Gen-SC control. It is evident from Eq. 8 that the force generated by the LPMG can be controlled with only q-axis current i_q. Therefore, i_q^{ref} is generated by using Eqs. (8), (31) and (32) as:

$$i_q^{ref} = -\frac{2\tau}{3\psi_{PM}} f_{pto}^{ref} \tag{33}$$

2) Controller design: The LPMG d- and q-axis currents are controlled via the Gen-SC. In this regard, i_d^{ref} is set to zero, to minimise generator losses, and i_q^{ref} is generated through Eq. (33) for maximum power extraction. To this end, the following error signals are introduced:

$$e_1 = x_1 - i_d^{ref} \tag{34}$$

$$e_2 = x_2 - i_q^{ref} \tag{35}$$

To achieve the control objectives detailed at the start of Section III, these errors must be regulated to zero. Using (26) and (27), the dynamics of e_1 and e_2 can be derived as:

$$\dot{e_1} = -\frac{R_s}{L_s}x_1 + \omega_e x_2 - \frac{1}{L_s}x_5\mu_d - \dot{i_d^{ref}} \tag{36}$$

$$\dot{e_2} = -\omega_e x_1 - \frac{R_s}{L_s}x_2 - \frac{\omega_e}{Ls}\psi_{PM} - \frac{1}{L_s}x_5\mu_q - \dot{i_q^{ref}} \tag{37}$$

To drive errors e_1 and e_2 to zero, $\dot{e_1}$ and $\dot{e_2}$ are forced to behave as:

$$\dot{e_1} = -c_1 e_1 \tag{38}$$

$$\dot{e_2} = -c_2 e_2 \tag{39}$$

where, $c_1 > 0$ and $c_2 > 0$, are design parameters. Comparing Eqs. (36), (37) to Eqs. (38), (39) results in the following control laws for the Gen-SC:

$$\mu_d = \frac{1}{x_5}[-R_s x_1 + \omega_e L_s x_2 + c_1 e_1 L_s - L_s \dot{i_d^{ref}}] \tag{40}$$

$$\mu_q = \frac{1}{x_5}[-\omega_e L_s x_1 - R_s x_2 - \omega_e \psi_{PM} + c_2 e_2 L_s - L_s \dot{i_q^{ref}}] \tag{41}$$

B. Control of the HESS converters

The second control objective is to regulate DC bus voltage using HESS. Direct DC bus voltage regulation is not possible due to the non-minimum phase nature of the buck-boost converters used with the HESS [22], so an indirect approach is needed here. Specifically, DC bus voltage regulation is achieved by forcing battery current x_3 to its reference I_{bat}^{ref}, which is generated through the energy management strategy (supervisory control) explained in Section IV. Hence, the following error is defined:

$$e_3 = x_3 - i_{bat}^{ref} \tag{42}$$

Using Eq. (28), the dynamics of e_2 are derived as:

$$\dot{e_3} = \frac{V_{bat}}{L_{bat}} - \frac{R_{bat}}{L_{bat}}x_3 - \mu_{45}\frac{x_5}{L_{bat}} - \dot{i_{bat}^{ref}} \tag{43}$$

To regulate this error to zero, e_3 is enforced to behave as:

$$\dot{e_3} = -c_3 e_3 + e_5 \tag{44}$$

where, $c_3 > 0$ is a design parameter. e_5 is now defined as the error between x_5 and V_{dc}^{ref}, as follows:

$$e_5 = x_5 - V_{dc}^{ref} \tag{45}$$

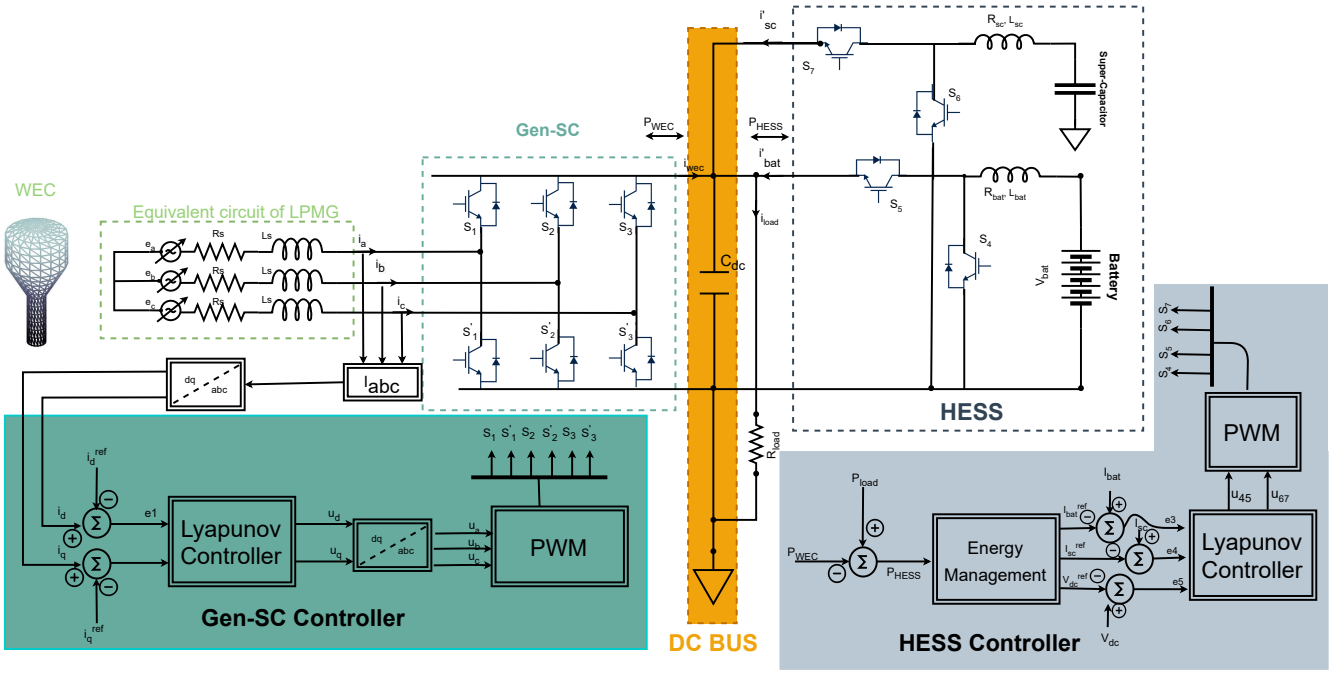

Fig. 2: A complete schematics of DC microgrid and its control

The control law μ_{45} is easily obtained by comparing (43) and (44) as:

$$\mu_{45} = \frac{L_{bat}}{x_5}[(\frac{V_{bat} - R_{bat}}{L_{bat}})x_3 + c_3 e_3 - e_5 - \dot{i_{bat}^{ref}}] \quad (46)$$

It is worth mentioning that e_5 is introduced in (46) as an extra damping term to adjust the output response. The dynamics of e_5 will be introduced later. For SC current tracking, the following error is introduced:

$$e_4 = x_4 - i_{sc}^{ref} \quad (47)$$

Taking the derivative of (47) and using (29) gives:

$$\dot{e_4} = \frac{V_{sc}}{L_{sc}} - \frac{R_{sc}}{L_{sc}} x_4 - \mu_{67}\frac{x_5}{L_{sc}} - \dot{i_{sc}^{ref}} \quad (48)$$

To achieve the control objective of SC current tracking, the error $\dot{e_4}$ should be decreasing, exponentially if possible, to zero.

$$\dot{e_4} = -c_4 e_4 \quad (49)$$

Comparing (48) and (49) yields the following control law:

$$\mu_{67} = \frac{L_{sc}}{x_5}[(\frac{V_{sc} - R_{sc}}{L_{sc}})x_3 + c_4 e_4 - \dot{i_{sc}^{ref}}] \quad (50)$$

C. Stability analysis

The stability of the closed loop system is established by using the Lyapunov stability criterion. This is done by investigating that the control laws defined in (40), (41), (46) and (50) are able drive the error system $(e_1, e_2, e_3, e_4, e_5)$ to zero. In this regard, a quadratic Lyapunov candidate function $V > 0$ is considered:

$$V = \frac{1}{2}(e_1^2 + e_2^2 + e_3^2 + e_4^2 + e_5^2). \quad (51)$$

For the system to be asymptotically stable, the derivative of V must be negative definite. Taking the derivative of (51) yields:

$$\dot{V} = (e_1\dot{e_1} + e_2\dot{e_2} + e_3\dot{e_3} + e_4\dot{e_4} + e_5\dot{e_5}) \quad (52)$$

Substituting expressions for $\dot{e_1}, \dot{e_2}, \dot{e_3}$, and $\dot{e_4}$ from (38), (39), (44) and (49), respectively, into (52) results in the following:

$$\dot{V} = -c_1 e_1^2 - c_2 e_2^2 - c_3 e_3^2 - c_4 e_4^2 + e_5(e_3 + \dot{e_5}) \quad (53)$$

Recall that the dynamics of e_5 have yet to be defined, the objective being to define $\dot{e_5}$ in such a way that it makes $\dot{V}$ negative definite i.e. $\dot{V} < 0$. To this end, $\dot{e_5}$ is forced to behave as:

$$\dot{e_5} = -c_5 e_5 - e_3 \quad (54)$$

where $c_5 > 0$ is a design parameter. Using (54), $\dot{V}$ is updated as :

$$\dot{V} = -c_1 e_1^2 - c_2 e_2^2 - c_3 e_3^2 - c_4 e_4^2 - c_5 e_5^2 \quad (55)$$

Eq. (55) shows that the $\dot{V} < 0$; hence, asymptotically stability of the equilibrium $(e_1, e_2, e_3, e_4, e_5) = (0, 0, 0, 0, 0)$, is achieved.

IV. Energy Management System

An energy management system (EMS) is used here for optimal power sharing between the components of the HESS i.e. battery and supercapacitor. The EMS is based on the power balance and fixed filter-based approach [23]. Fig. 3 shows the EMS implemented in this study. The EMS serves three purposes: (i) first, it provides reference battery and SC currents for the Lyapunov (low level) controller (ii) secondly, it decreases stress on the battery by using the SC during

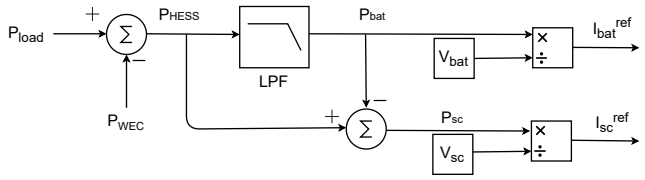

Fig. 3: Energy management system

high frequency power exchange, and (iii) thirdly, it also ensures power balance at the DC bus under variable generation and load. The power balance at the DC microgrid is expressed as follows:

$$P_{HESS}^{req} = P_{load} - P_{WEC} = V_{dc}^{ref}(i_{load} - i_{wec}) \quad (56)$$

where, P_{WEC} and P_{load} are the WEC and load power, respectively. P_{HESS}^{req} is the required power from the storage. The EMS converts P_{HESS}^{req} into two components using a low pass filter (LPF). Low frequency components of required power are used to generate the battery reference current I_{bat}^{ref}, whereas high frequency components generate the SC reference current I_{sc}^{ref}, as shown in Fig. 3. The generated references are then fed into the respective Lyapunov controllers for battery and SC converters.

V. Simulation results

TABLE I: System parameters for the simulation study

WEC	
Total mass M	1.4646×10^5 kg
Hydrostatic stiffness K_{hs}	5.5724×10^5 N/m
Wave period T_p	8.3752 s
LPMG and Gen-SC	
Stator Resistance R_s	0.29 Ω
Stator inductance L_s	0.03 H
Flux linkage ψ_{PM}	23 Wb
Pole pitch τ	0.1 m
Controller gains	c_1 = 9×10^4, c_2 = 3×10^6
HESS and DC/DC converters	
Battery bank	540 v, 70Ah
Supercapacitor	550v, 350F
Inductance L_{bat}, L_{sc}	3.3 mH, 3.3 mH
ESRs R_{bat}, R_{sc}	20 mΩ, 20 mΩ
Controller gains	c_3 = 100, c_4 = 3×10^3, c_5 = 1×10^6
DC bus	
Voltage V_{dc}^{ref}	1000 v (RL), 1500 v (ACC)
Capacitance C_{dc}	4 mF

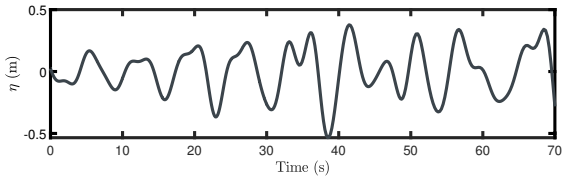

Fig. 4: Incident wave profile, $H_s = 1$ m and $T_p = 8.3752$ s

The performance of the proposed scheme is evaluated by simulations performed in the MATLAB/Simulink environment. The parameters of the simulated system are given in Table I. A full-scale CorPower-like device is considered, and the WEC dimensions are based upon the study presented in [24]. An irregular wave model is considered in this study, generated from a Pierson-Moskowitz (PM) spectrum [25], with significant wave height $H_s = 1$ m and period $T_p = 8.3752$ s, as shown in Fig. 4.

The tracking performance of the Lyapunov based controller is illustrated in Fig. 5 with passive hydrodynamic control. Figs. 5a, 5b and 5c show the tracking performance of the Gen-SC controllers (u_d, u_q), which show perfect convergence of f_{pto}, i_q and i_d to their respective references under variable wave forcing. Figs. 5d-5f present the tracking performance of the HESS converter controllers (μ_{45}, μ_{67}), which is quite satisfactory. It is evident that i_{sc} contains only high frequency components, while i_{bat} contains relatively low frequency components of required current from the HESS, according to the EMS allocation. This reduces stress on the battery and increases battery lifetime. The DC bus voltage V_{dc}^{bus} is tightly regulated for this case and settles quickly to the constant reference voltage. It is important to mention that the PTO force reference generated from passive damping for maximum power extraction is not a great choice, due to its limited power extraction capability. However, it has some benefits from a grid integration perspective, due to unidirectional power flow requirement.

Fig 6 shows the performance of the proposed controller with ACC hydrodynamic control. The tracking performance of the proposed controller for Gen-SC is also satisfactory for this case. It is evident, from Fig. 6a, that the amplitude of the PTO force f_{pto} is much higher (almost 4 times) than RL control for the same wave profile. This behaviour is also reflected in the q-axis current of the LPMG in Fig. 6b, which is increased substantially for ACC control. The increased power output from the WEC under ACC hydrodynamic control has implications for the LPMG, power converters and storage system, in terms of power ratings and equipment costs. Furthermore, ACC involves the production of higher output voltages and currents at generator terminals, which leads to higher DC bus voltage requirements. Figs. 6d, 6e and 6f indicate the tracking performance of the HESS converter control, and show good tracking. It is also noted that, at higher current levels, the battery current and dc bus voltage show some departure from the reference point, as shown in Fig. 7, but these variations are very low and fairly acceptable.

It is important to note that the results shown in Figs. 5 and 6 are for a constant load on the DC microgrid. To validate the performance under variable load, simulations are performed for sudden load changes as shown in Fig. 8. Fig. 9 shows the DC bus voltage regulation under sudden load changes and it is clear that the proposed controller is able to compensate for these load changes. Hence, DC bus voltage regulation is achieved under both variable generation and changes in load.

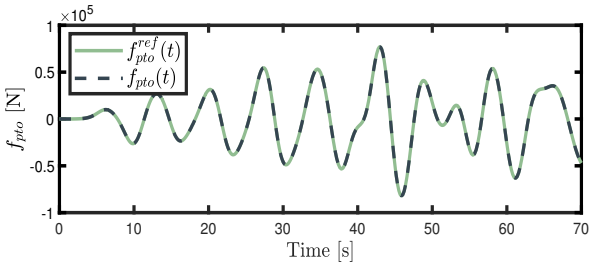

(a) PTO force

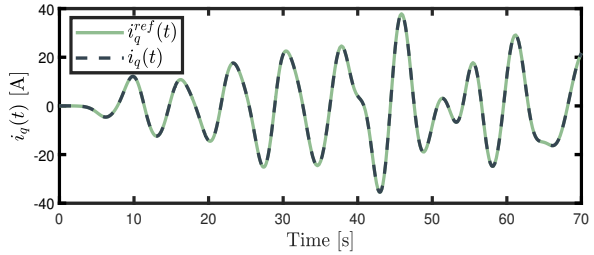

(b) LPMG q-axis current

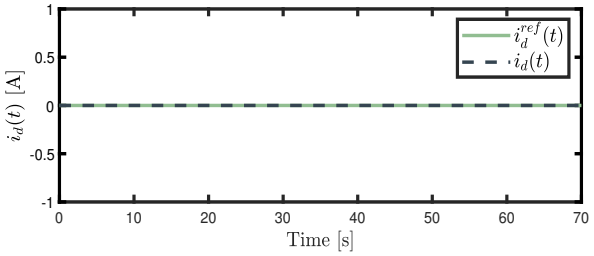

(c) LPMG d-axis current

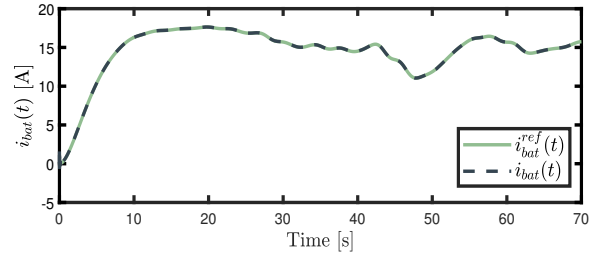

(d) Battery current

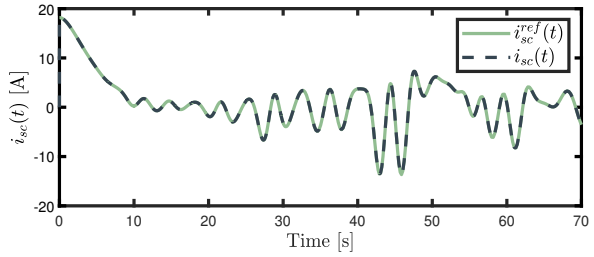

(e) SC current

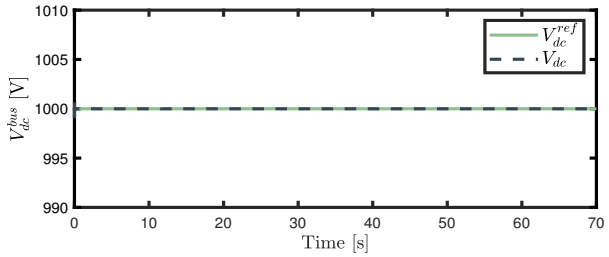

(f) DC bus voltage

Fig. 5: Tracking performance of the proposed controller under passive hydrodynamic control (RL control)

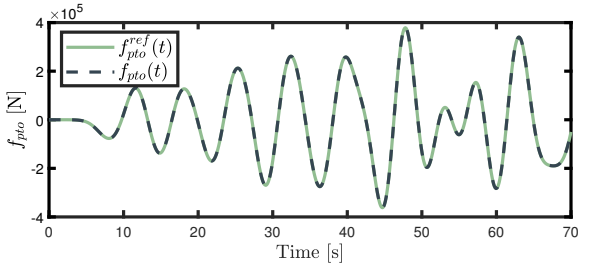

(a) PTO force

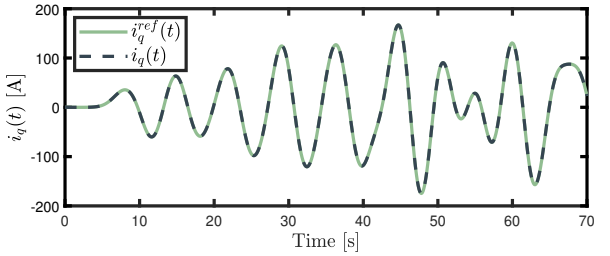

(b) LPMG q-axis current

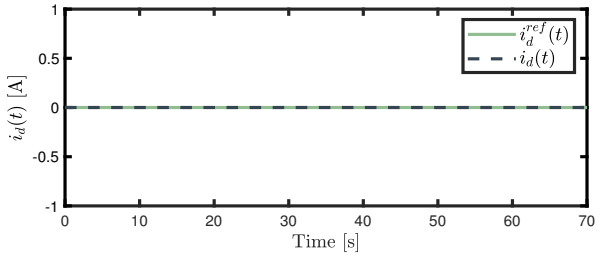

(c) LPMG d-axis current

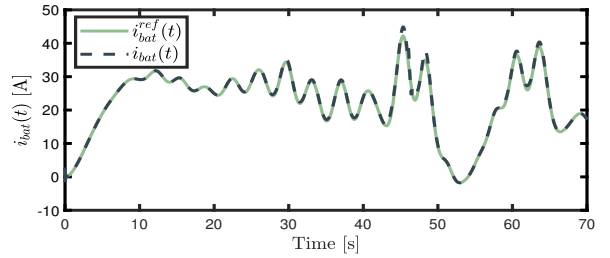

(d) Battery current

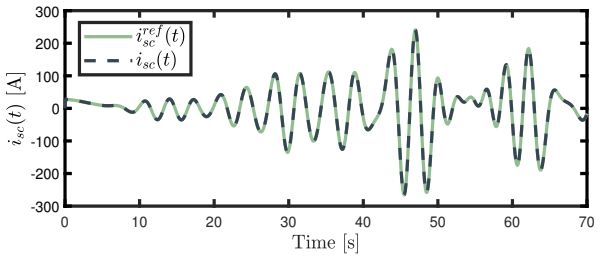

(e) SC current

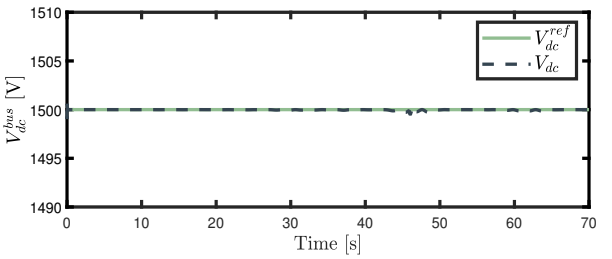

(f) DC bus voltage

Fig. 6: Tracking performance of the proposed controller under reactive hydrodynamic control (ACC control)

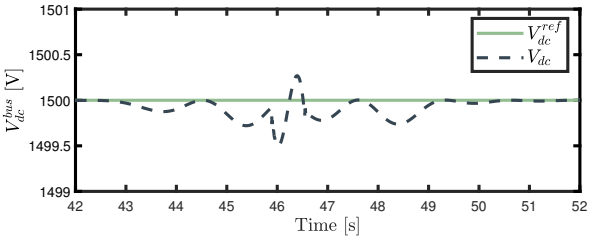

Fig. 7: DC bus voltage (zoomed in)

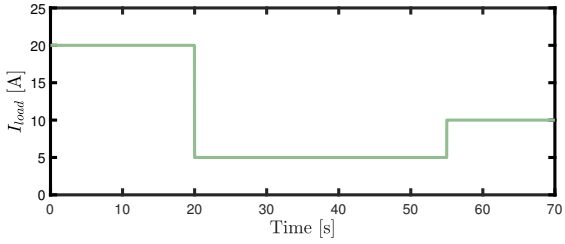

Fig. 8: DC load variations

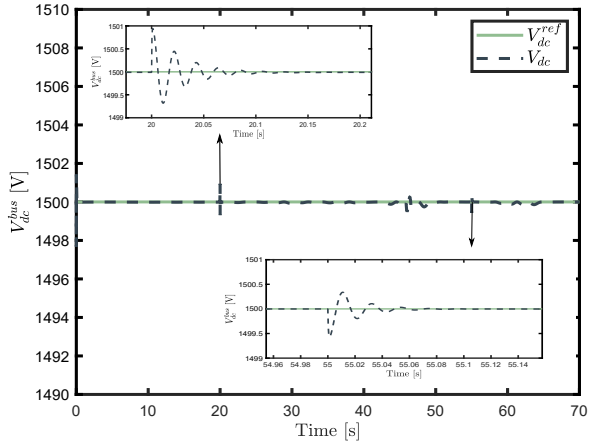

Fig. 9: DC bus voltage for sudden load changes

VI. Conclusions

In this paper, Lyapunov based control is proposed for a DC microgrid using wave energy as a RES. Maximum power extraction from waves is achieved through the control of Gen-SC, using hydrodynamic control (RL and ACC). DC bus voltage regulation is achieved under variable generation and load, with the help of an actively controlled HESS. An EMS is also used to ensure optimal power-sharing between the components of the HESS. Stability analysis is carried out using Lyapunov stability criteria for the proposed system, which guarantees the microgrid's asymptotic stability. The performance of the proposed framework is studied by simulation in the MATLAB/Simulink environment, and results show the proposed controller works well under both variable generation and load.

It can also be concluded that the choice of hydrodynamic control will have implications on the overall cost and operational range of the system. ACC control gives more power than RL control; however, ACC produces significantly higher output power peaks, leading to higher ratings (costs) for the electrical and storage equipment. Moreover, every component in the power train has operational constraints, which are also affected by the choice of hydrodynamic control, although more advanced hydrodynamic control algorithms can actively optimise operation within such physical constraints.

Acknowledgement

Thanks are due to CarrieAnne Barry of the Centre for Ocean Energy Research (COER) at Maynooth University for providing language help and proof reading the article. This work is supported by COER and the Dept. of Electronic Engineering, Maynooth University, and by Science Foundation Ireland through the Marine Renewable Ireland (MaREI) Centre under Grant 12/RC/2302.

References

[1] S. Ullah, A. M. A. Haidar, P. Hoole, H. Zen, and T. Ahfock, "The current state of Distributed Renewable Generation, challenges of interconnection and opportunities for energy conversion based DC microgrids," *J. Clean. Prod.*, p. 122777, 2020.

[2] Q. Xu, N. Vafamand, L. Chen, T. Dragičević, L. Xie, and F. Blaabjerg, "Review on Advanced Control Technologies for Bidirectional DC/DC Converters in DC Microgrids," *IEEE J. Emerg. Sel. Top. Power Electron.*, 2020.

[3] J. Peng, B. Fan, and W. Liu, "Voltage-Based Distributed Optimal Control for Generation Cost Minimization and Bounded Bus Voltage Regulation in DC Microgrids," *IEEE Trans. Smart Grid*, 2020.

[4] I. López, J. Andreu, S. Ceballos, I. M. de Alegr'ia, and I. Kortabarria, "Review of wave energy technologies and the necessary power-equipment," *Renew. Sustain. Energy Rev.*, vol. 27, pp. 413–434, 2013.

[5] H. Polinder and M. Scuotto, "Wave energy converters and their impact on power systems," in *2005 Int. Conf. Futur. Power Syst.* IEEE, 2005, pp. 9—pp.

[6] A. Blavette, D. L. O'Sullivan, A. W. Lewis, and M. G. Egan, "Impact of a wave farm on its local grid: Voltage limits, flicker level and power fluctuations," in *2012 Ocean.* IEEE, 2012, pp. 1–9.

[7] S. Armstrong, D. Mollaghan, and R. Alcorn, "Effect of wave farm aggregation on power system stability," in *2014 IEEE 5th Int. Symp. Power Electron. Distrib. Gener. Syst.* IEEE, 2014, pp. 1–6.

[8] W. Jing, C. H. Lai, S. H. W. Wong, and M. L. D. Wong, "Battery-supercapacitor hybrid energy storage system in standalone DC microgrids: a review," *IET Renew. Power Gener.*, vol. 11, no. 4, pp. 461–469, 2016.

[9] S. Zhang, R. Xiong, and J. Cao, "Battery durability and longevity based power management for plug-in hybrid electric vehicle with hybrid energy storage system," *Appl. Energy*, vol. 179, pp. 316–328, 2016.

[10] H. Armghan, M. Yang, M. Q. Wang, N. Ali, and A. Armghan, "Nonlinear integral backstepping based control of a DC microgrid with renewable generation and energy storage systems," *Int. J. Electr. Power Energy Syst.*, vol. 117, p. 105613, 2020.

[11] S. Rasool, M. R. Islam, K. M. Muttaqi, and D. Sutanto, "Coupled Modeling and Advanced Control for Smooth Operation of a Grid-Connected Linear Electric Generator Based Wave-to-Wire System," *IEEE Trans. Ind. Appl.*, vol. 56, no. 5, pp. 5575–5584, 2020.

[12] H. M. Hasanien, "Gravitational search algorithm-based optimal control of Archimedes wave swing-based wave energy conversion system supplying a DC microgrid under uncertain dynamics," *IET Renew. Power Gener.*, vol. 11, no. 6, pp. 763–770, 2016.

[13] M. R. Adaryani, S. A. Taher, and J. M. Guerrero, "Model predictive control of direct-drive wave power generation system connected to DC microgrid through DC cable," *Int. Trans. Electr. Energy Syst.*, vol. 30, no. 9, p. etep12484, 2020.

[14] W. E. Cummins, "The impulse response function and ship motions," David Taylor Model Basin Washington DC, Tech. Rep., 1962.

[15] N. Faedo, Y. Peña-Sanchez, and J. V. Ringwood, "Finite-order hydrodynamic model determination for wave energy applications using moment-matching," *Ocean Eng.*, vol. 163, pp. 251–263, 2018.
[16] B. Guo, R. J. Patton, S. Jin, and J. Lan, "Numerical and experimental studies of excitation force approximation for wave energy conversion," *Renew. Energy*, vol. 125, pp. 877–889, 2018.
[17] J. S. Park, B.-G. Gu, J. R. Kim, I. H. Cho, I. Jeong, and J. Lee, "Active phase control for maximum power point tracking of a linear wave generator," *IEEE Trans. Power Electron.*, vol. 32, no. 10, pp. 7651–7662, 2016.
[18] A. El Magri, F. Giri, G. Besancon, A. El Fadili, L. Dugard, and F. Z. Chaoui, "Sensorless adaptive output feedback control of wind energy systems with PMS generators," *Control Eng. Pract.*, vol. 21, no. 4, pp. 530–543, 2013.
[19] Z. Xu, D. Zhang, F. Wang, and D. Boroyevich, "A unified control for the combined permanent magnet generator and active rectifier system," *IEEE Trans. Power Electron.*, vol. 29, no. 10, pp. 5644–5656, 2014.
[20] A. de la Villa Jaén, A. G. Santana, and Others, "Considering linear generator copper losses on model predictive control for a point absorber wave energy converter," *Energy Convers. Manag.*, vol. 78, pp. 173–183, 2014.
[21] A. de la Villa Jaén, A. Garc'ia-Santana, and D. E. Montoya-Andrade, "Maximizing output power of linear generators for wave energy conversion," *Int. Trans. Electr. Energy Syst.*, vol. 24, no. 6, pp. 875–890, 2014.
[22] H. El Fadil and F. Giri, "Backstepping based control of PWM DC-DC boost power converters," in *2007 IEEE Int. Symp. Ind. Electron.* IEEE, 2007, pp. 395–400.
[23] S. Hazra and S. Bhattacharya, "Hybrid energy storage system comprising of battery and ultra-capacitor for smoothing of oscillating wave energy," in *2016 IEEE Energy Convers. Congr. Expo.* IEEE, 2016, pp. 1–8.
[24] J. H. Todalshaug, G. S. Ásgeirsson, E. Hjálmarsson, J. Maillet, P. Möller, P. Pires, M. Guérinel, and M. Lopes, "Tank testing of an inherently phase-controlled wave energy converter," *International Journal of Marine Energy*, vol. 15, pp. 68–84, 2016.
[25] W. J. Pierson Jr and L. Moskowitz, "A proposed spectral form for fully developed wind seas based on the similarity theory of SA Kitaigorodskii," *J. Geophys. Res.*, vol. 69, no. 24, pp. 5181–5190, 1964.